Forensic Science International 248 (2015) 148–153

Contents lists available at ScienceDirect

Forensic Science International

journal homepage: www.elsevier.com/locate/forsciint

Assessment of fiducial markers to enable the co-registration of photographs and MRI data

Bridgette A. Webb [a,*], Andreas Petrovic [a,b], Martin Urschler [a,c], Eva Scheurer [a,d]

[a] Ludwig Boltzmann Institute for Clinical Forensic Imaging, Graz, Austria
[b] Institute of Medical Engineering, BioTechMed, Graz University of Technology, Austria
[c] Institute for Computer Graphics and Vision, BioTechMed, Graz University of Technology, Austria
[d] Institute of Forensic Medicine, Medical University Graz, Austria

ARTICLE INFO

Article history:
Received 13 November 2014
Accepted 29 December 2014
Available online 16 January 2015

Keywords:
Soft tissue injuries
MRI
Fiducial markers
Forensic medicine
Multi-modal co-registration

ABSTRACT

Purpose: To investigate the visualisation of novel external fiducial skin markers in photography and MRI. To co-register photographs and MR images, and additionally assess the spatial accuracy of these co-registrations with the view of future application in the investigation of forensically relevant soft tissue lesions.

Methods and materials: Strand-shaped fiducial markers were secured externally over hematomas on the thigh of 10 volunteers. The region of interest was photographed and examined using MRI at 3 T in oblique and transversal orientations and the visibility of the markers assessed. Markers provided 'control points' in both sets of images, enabling the computation of an affine transform to register oblique MR images to photographs. The fiducial registration error was evaluated by calculating the root-mean-square error of nine corresponding evaluation points visible in both modalities.

Results: Fiducial markers were clearly visualised in both photography and MRI. The co-registration of photographs and oblique MR images was achieved for all participants. The overall root-mean-square error for registrations was 1.18 mm (TIRM) and 1.46 mm (TSE2D with SPAIR fat-suppression).

Conclusions: The proposed approach led to the successful visualisation of non-invasive fiducial markers using photography and MRI (TIRM and TSE2D (SPAIR) sequences). This visualisation, combined with an affine transformation process provided a simple, cost-effective way to accurately co-register photographs and MR images of subcutaneous hematomas located on the thigh. Further investigation of the novel markers and the proposed co-visualisation approach holds potential to improve not only the forensic documentation of soft tissue lesions, but to also improve certain clinical applications, including the area of dermatology.

1. Introduction

Due to its excellent contrast, multi-planar capability and radiation-free nature, meaning that no tissue-ionizing radiation is involved, Magnetic Resonance Imaging (MRI) has become a well-established modality for the detection and evaluation of soft tissue lesions [1,2]. In the context of forensic medicine, it has also shown particular utility in the detection and assessment of trauma-induced subcutaneous soft tissue lesions, including subcutaneous cavities, localized disruptions, large-scale tissue disintegration and décollement-like lesions [3]. Furthermore, the forensic detection and evaluation of such lesions requires the inclusion of externally visible findings due to the proximity of these injuries to the skin surface. The accurate correlation of externally visible damage, such as bruising, with internal lesions visualised in MRI can deliver a more complete expert interpretation of the injuries observed and potentially enables sophisticated visualisation techniques for presenting details of forensic interest in the context of person-specific 3D models [15]. Through the co-registration [4] of images, the spatial relationship between photographs and MRI data can be established. Mapping these images to one another creates a single, simultaneous representation of data coming from two different sources. Furthermore, co-registration improves the visualisation of multiple lesions in the same area by displaying the connection between findings detected in MRI and those visible in photographs. Thereby, the comprehensibility of complex medical imaging

Abbreviations: SPAIR, spectrally attenuated inversion recovery; TIRM, turbo inversion recovery magnitude; BI, base image; RMSE, root-mean-square error.

* Corresponding author at: Ludwig Boltzmann Institut für Klinisch-Forensische Bildgebung, Universitätsplatz 4/2, Graz 8010, Austria. Tel.: +43 316 380 7721.
E-mail address: bridgette.webb@cfi.lbg.ac.at (B.A. Webb).

http://dx.doi.org/10.1016/j.forsciint.2014.12.027
0379-0738/

material in a court of law is notably improved. For example, in a sexual assault case, where bruising of the inner thigh is a common finding [5], photographs demonstrating the location of bruising, and MRI data, providing additional internal information such as the depth and underlying shape of the bruises can be co-visualised. This provides a layperson with a fuller picture of the injuries obtained and enables a better understanding of the extent of these injuries.

In clinical practice, the co-registration of multi-modal images is currently achieved through the use of anatomical landmarks or through fiducial markers. Not all body regions contain appropriate anatomical landmarks. This is especially problematic in the forensic assessment of subcutaneous soft tissue, where no such landmarks can be found. To address the lack of anatomical landmarks in certain regions, spherical or ellipsoidal external skin markers including lipid markers [6], vitamin E capsules [7], fish oil capsules [8] or point-based commercial markers [9] have been introduced. Nevertheless, these skin markers often cannot be applied in forensically relevant MR examinations of subcutaneous tissue, as they can produce artefacts in the MR images which then interfere with the forensic assessment of findings in the region.

To address this problem, a novel array of strand-shaped fiducial skin markers and corresponding visualisation technique were assessed in the present study. The strand-shaped nature of the markers was based on fiducial markers previously found to be effective in registering MR and histology images of the prostate [10]. Compatibility of the proposed markers with MRI sequences [11,12] currently used to visualise subcutaneous hematomas was important considering the intended forensic application of the proposed technique.

The objectives of this study were as follows:

(1) To establish a technique for the reliable documentation and visualisation of external fiducial skin markers in photography and MRI;
(2) To investigate the visibility of the fiducial markers in these modalities; and
(3) To co-register the acquired images through the application of an affine transformation function and assess the spatial accuracy of the resultant co-registrations.

More broadly, the present study aims to contribute to the improved detection and documentation of forensically relevant lesions in superficial soft tissue through the co-registration of multi-modal images.

2. Materials and methods

2.1. Subjects

This prospective study was conducted with the approval of the local university ethics committee and the informed consent of all participants. Ten Caucasian volunteers (median age 26.3 years, range 25.1–33.9 years, 2(m)/8(f)) with at least one externally visible hematoma on their thigh were included in the study.

2.2. Fiducial markers

The fiducial skin markers used in this study were cotton threads (diameter: approximately 2 mm, 100% cotton, black) soaked in commonly available corn oil.

2.3. Documentation and visualisation of markers

Markers were secured over the hematoma using a transparent medical patch (Fig. 1), which enabled the reliable documentation of both the position of the markers and the externally visible characteristics of the hematomas. The region of interest was photographed before and after MR imaging. For all participants, MR images were acquired in transverse and oblique orientations using three sequences known to visualise subcutaneous soft tissue lesions [11,12] (see details in Table 1) and using one of two 4-channel CPC coil elements (Noras GmbH, Germany) at 3 T (TimTrio or Skyra, Siemens AG, Germany). To best visualise markers and produce images in a plane similar to that of the photographs, the oblique imaging plane was aligned as well as possible with the skin surface.

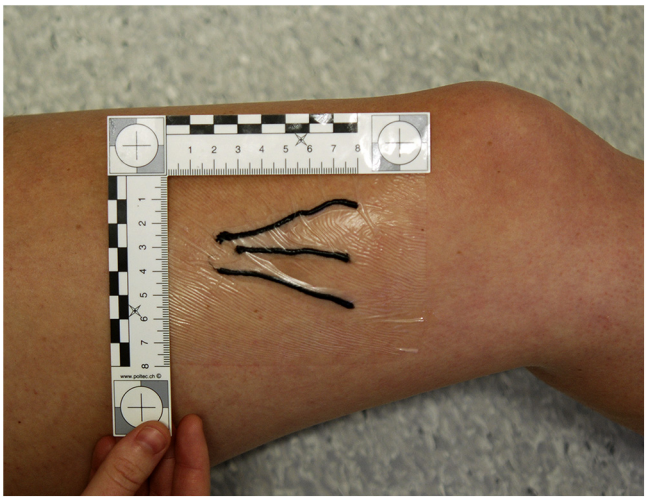

Fig. 1. Marker placement and fixation over a hematoma on the thigh. Creation of base image (BI).

2.4. Visibility assessment

A visual assessment of the markers in the photographs and MR images acquired was performed. The usefulness of the images was further evaluated based on the ease with which so-called registration 'control points' could be located. Such 'control points' were marker particularities e.g. the ends and curves of markers. Their identification was essential to the registration process.

2.5. Image registration

Corresponding 'control points' were manually identified in the photographs and oblique MR images acquired at the skin surface. From these points, a transformation matrix was extracted (*cp2tform*, Matlab, R2012b), and an affine transformation with bicubic interpolation was applied to register MR images to the

Table 1
Sequence parameters used for the acquisition of MR images in oblique and transversal orientations.

	TIRM	TSE2D	TSE-PDw
Orientation	Oblique	Oblique	Transversal
TE (ms)	12	10	12
TR (ms)	7000	1540	3290
Slice thickness (mm)	1.5	1.5	1.5
In-plane resolution (mm)	0.52	0.52	0.52
Flip angle	–	150°	136°
Fat-suppression	TI200	SPAIR	SPAIR
Bandwidth (Hz/px)	200	223	223

*TE = Echo Time, TR = Repetition Time, TIRM = Turbo Inversion Recovery Magnitude, TSE = Turbo Spin Echo, TI = Inversion Time, SPAIR = Spectrally Attenuated Inversion Recovery.

BI (photograph of lesion with markers in place, Fig. 1). Visual assessment of registrations was performed by varying the image opacity of the registration to examine the quality of each registration. If necessary, additional 'control points' were selected and the images re-registered before progressing to the application of transformation parameters to oblique scans acquired deeper in the subcutaneous tissue.

2.6. Spatial accuracy of the co-registration

The error of the proposed fiducial registrations was computed for all participants individually by comparing the coordinates of nine corresponding evaluation points in both modalities. The positions of three transversal MRI slices (approx. 7.5 mm apart) were overlaid onto the oblique images (Syngo work station imaging software, Siemens AG, Germany). The nine intersections of the markers and the transversal slice markings were taken as the evaluation points. The abovementioned affine transformation was applied to the overlays as well as to the MR images to display their positions on photographs and registered MR images (Fig. 2).

The difference in the coordinates of the nine points (Δx and Δy) at which these lines intercepted with the markers was used to compare the spatial accuracy of registrations with the base images (BI) (Eq. 1).

$$\begin{pmatrix} \Delta X \\ \Delta Y \end{pmatrix} = \begin{pmatrix} X \\ Y \end{pmatrix}_{\mathrm{MRI}} - \begin{pmatrix} X \\ Y \end{pmatrix}_{\mathrm{BI}} \quad (1)$$

The root-mean-square error ($\mathrm{RMSE_{ind}}$) for a certain sequence and participant was given by the equation

$$\mathrm{RMSE_{ind}} = \sqrt{\frac{1}{n}\sum_{i=1}^{n}(\Delta x_i^2 + \Delta y_i^2)}, \quad (2)$$

where n, the number of intersecting points on a given registered MR image and corresponding BI, was 9.

For both fat-suppression techniques, the overall RMSE ($\mathrm{RMSE_{overall}}$) was given by statistically pooling the previously calculated individual RMSEs ($\mathrm{RMSE_{ind}}$) according to the equation

$$\mathrm{RMSE_{overall}} = \sqrt{\frac{1}{p}\sum_{i=1}^{p}(\mathrm{RMSE_{ind}^2})}, \quad (3)$$

where p was the number of participants.

3. Results

3.1. Visibility

The external markers were clearly visible in both modalities (photography and MRI) assessed in the present study. Furthermore, in the MRI sequences applied, hematomas were also visible, presenting as bright against the fat-suppressed signal of the subcutaneous soft tissue.

Use of a transparent medical patch and black markers ensured excellent contrast between markers and skin in photographs (Fig. 1). The signal from the external markers was consistently visible in each of the MRI sequences employed in the present study (Fig. 4(c,f)). In the oblique sequences, a dark signal void was observed in slices corresponding to the physical position of the markers (Fig. 3b), while markers appeared hyperintense in the slices preceding the position of the 'real' marker (i.e. above the markers). When imaging commenced slightly above the skin, surface markers presented as bright with excellent contrast against the dark background, i.e. air (Fig. 3a). In transversal images acquired, markers also appeared bright. Both oblique sequences produced images which allowed the identification of the previously mentioned 'control points' required for co-registration.

Through a better visualisation of the fiducial markers, the TIRM sequence facilitated the identification of such points (Fig. 4f). However, the TSE2D sequence with SPAIR fat-suppression resulted in a visibly better contrast between the lesion and surrounding tissue (Fig. 4d).

3.2. Image registration and spatial accuracy

Separate image registration was performed for each of the oblique sequences (for example, see Fig. 4). Overall, RMSEs of 1.18 mm for registrations using TIRM images, and 1.46 mm for those acquired using TSE2D with SPAIR fat-suppression were obtained (Table 2, Fig. 5).

4. Discussion

As outlined in the objectives, the present study established a technique for the documentation and visualisation of external strand-shaped fiducial markers. Both the visibility of these markers in photography and MRI, as well as their suitability to assist in the co-registration of images originating from these two

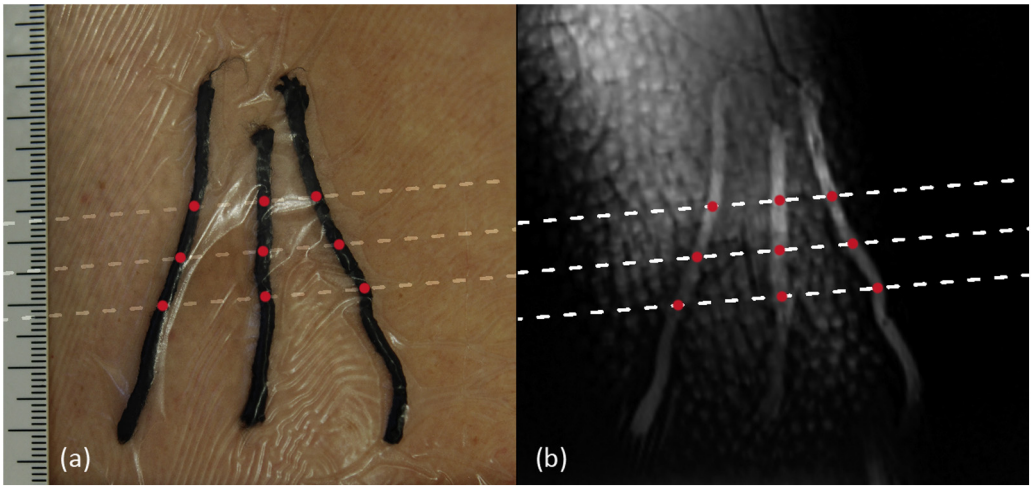

Fig. 2. Example of Fiducial registration error evaluation: Selection of 9 corresponding evaluation points in the photograph and registered MR image. Points located at the intercepts of markers and 3 transversal slices (approx. 7.5 mm apart).

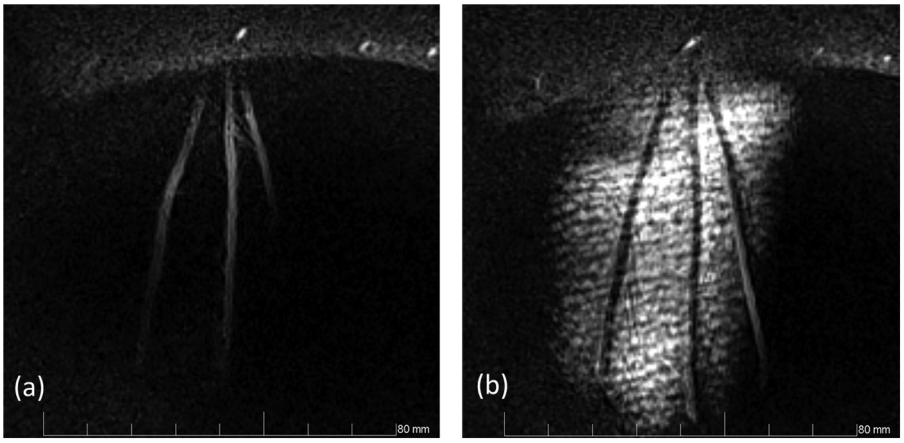

Fig. 3. Two consecutive TIRM slices depicting markers near the skin surface: (a) hyperintense signal and (b) partial signal void.

modalities was assessed. Photographs and MR images were successfully co-registered and the spatial accuracy of these co-registrations was determined.

4.1. Fiducial marker and hematoma visualisation

Following a brief pre-study investigation, corn oil was found to be an appropriate soaking agent due to the visibility of its fat signal in MRI and its retention by the cotton thread, which formed the marker basis.

The black fiducial markers applied in the present study were clearly visible against the skin of all ten subjects. The markers were additionally visualised in MRI using both a TIRM sequence and a TSE2D sequence with SPAIR fat-suppression (Table 1). The successful visualisation of the markers in the presence of fat-suppression techniques can be ascribed to the difference in the MR

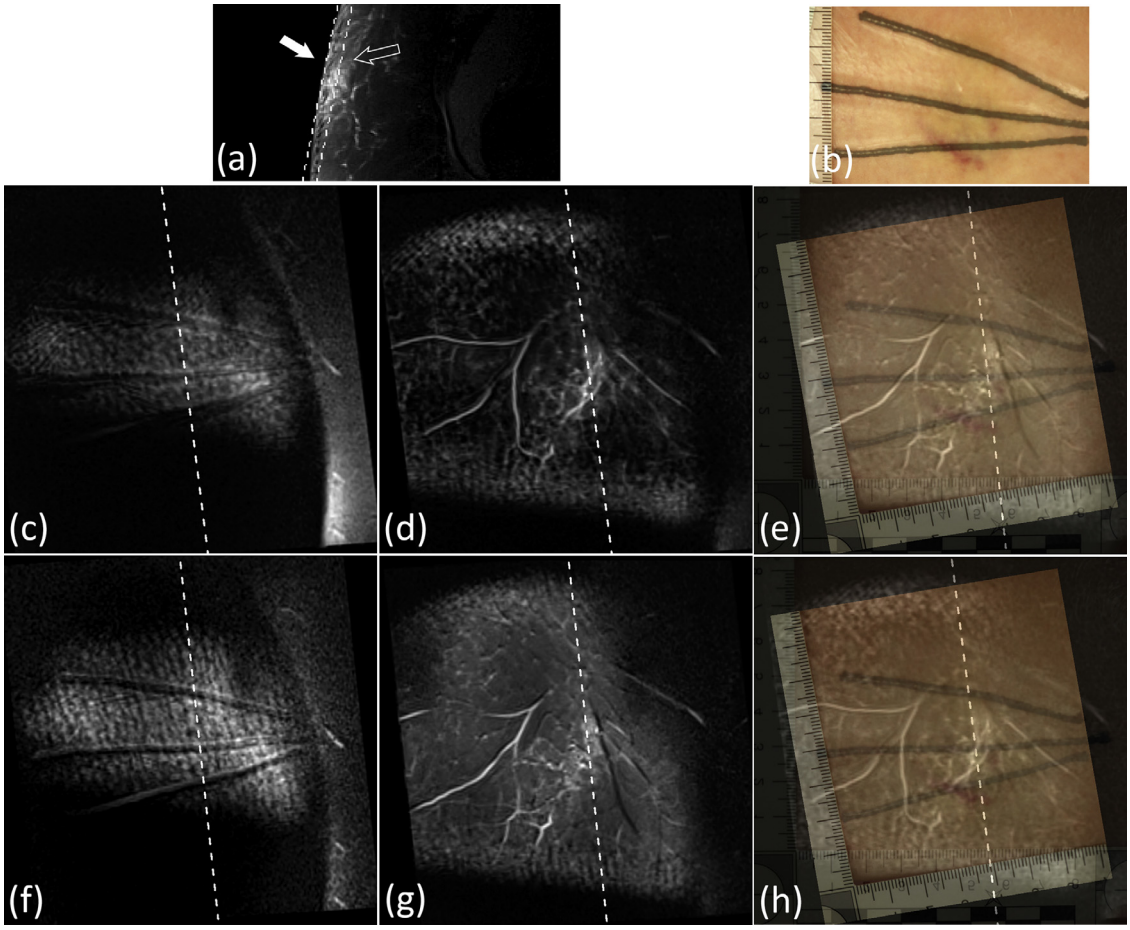

Fig. 4. (a) Transversal MR image displaying the positions of two oblique slices acquired at the skin surface (solid arrow) and in the subcutaneous fatty tissue (non-solid arrow). (b) Photograph of markers and lesion. (c) Sum of two oblique TSE2D (SPAIR) images acquired at the skin surface and registered to spatially correspond to the BI. All three fiducial skin markers are visible (dashed line indicates the relative position of the transversal slice (a)). (d) TSE2D (SPAIR) image acquired in the subcutaneous fatty tissue and registered to spatially correspond to the BI. Hematoma discernible from surrounding tissue (dashed line indicates the relative position of the transversal slice (a)). (e) Co-visualisation of MR image (TSE2D (SPAIR)) and photographs documenting the external findings. Images (f)–(h) correspond to the TIRM image equivalents of (c)–(e).

Table 2
Individual and overall RMSE (mm) for registered MR images (TIRM (TI = 200) and TSE SPAIR fat-suppression) relative to BI.

Participant	TIRM	TSE2D (SPAIR)
1	NA	1.36
2	1.32	2.94
3	0.79	1.63
4	0.85	0.55
5	1.95	0.72
6	1.06	1.27
7	0.45	0.54
8	1.99	2.07
9	0.26	0.75
10	0.58	0.69
Overall	1.18	1.46

signal originating in the corn oil markers compared to that generated by subcutaneous fat. This difference, caused by variation in the types and abundances of fatty acids present [13,14], led to a different fat-suppression efficiency in the markers compared to in subcutaneous fat. Consequently, the acquisition of oblique images at the skin surface, in which fiducial markers were visible, and the suppression of the majority of the subcutaneous fat signal were possible using both the TIRM and TSE2D (SPAIR fat-suppression) sequences.

The sequences proposed in the literature [11,12] not only enabled the successful visualisation of the fiducial markers in the present study, but were also suitable for the depiction of subcutaneous soft tissue hematomas in MRI. Using these sequences, the presence of the investigated fiducial markers did not interfere with the visualisation of underlying hematomas, which were visible using both the TIRM and TSE2D (SPAIR) sequences. Enhanced fat-suppression of the subcutaneous fatty tissue by the TSE2D sequence with SPAIR fat-suppression resulted in the observation of visibly superior contrast between hematomas and surrounding tissue in the images acquired with this sequence, compared to those acquired using the TIRM sequence.

4.2. Observed MRI artefacts

Since the fat signal originating in the markers was only minimally suppressed, a chemical shift artefact was observed in both the frequency encoding direction and the slice direction. While this artefact is commonly observed in the frequency encoding direction, it is generally minimal in the slice direction and often not visible. However, in the present study a hyperintense signal in the oblique slice preceding the real position of the markers, and a partial signal void in the slice corresponding to the actual position of the marker was observed. The combination of the slice selection bandwidth, a concentrated lipid source and a slice thickness smaller than the cross-section of the marker created conditions in which the fat signal misregistration was easily discernible. From simulations of the sequence, the slice selection bandwidth was determined to be 500 Hz, corresponding to a displacement of almost one slice thickness (1.3 mm). This effect was observed in the slice encoding direction regardless of if the oblique images were acquired moving into or out of the tissue. However, it had very little practical influence on the registration of images, which was nevertheless spatially accurate.

4.3. Image registration and spatial accuracy

The calculated registration error in both sets of registrations, i.e. using TIRM and SPAIR, was small and confirmed initial visual observations of the resultant co-visualisations. The image registration approach required the manual identification of corresponding 'control points' in MR images and photographs (e.g. marker curves and other particularities). By considering the ease with which these points could be identified, as well as the visual quality of the resultant registrations, it emerged that the TIRM images allowed the most efficient registration as marker contours were more clearly visible, due to the less effective fat-suppression and the better contrast between the markers and background. These initial observations were further confirmed by examination of the RMSE, which was slightly greater for the registrations performed using the SPAIR fat-suppressed images than for the TIRM images.

Ultimately, the choice between the two sequences should be based on the registration accuracy required and the suspected lesion to be investigated in the soft tissue. Registration using TIRM images was more accurate and less time consuming due to the facilitated identification of 'control points', however, SPAIR fat-suppression delivered superior contrast between hematomas and surrounding fatty tissue.

4.4. Factors influencing the spatial accuracy of the co-registration

The chemical shift artefact observed in the frequency encoding direction may have partially contributed to the overall fiducial registration error of the technique through a displacement of the position of the markers within the plane used to register the images. However, in the slice direction such displacement was perpendicular to the imaging plane, and, thus, did not contribute to the fiducial registration error. Accurate 'control point' selection was essential in the proposed image registration framework.

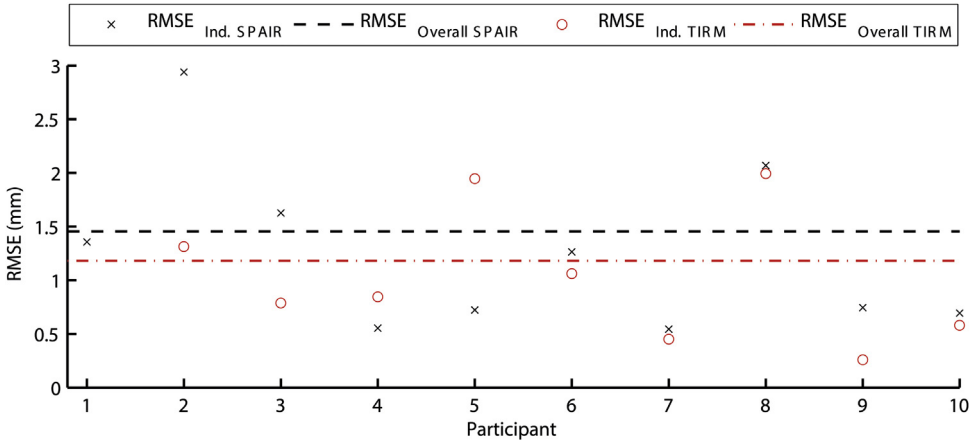

Fig. 5. Individual and overall RMSE of co-registrations.

Selection was found to be easiest at the curves and particularities of the markers, specifically the ends of the markers, meaning the correct positioning of the oblique imaging plane and the field of view (FOV) played a significant role. In certain cases, namely for the examination of very large hematomas and those located on uneven surfaces, the assumption that the FOV was planar over the entire lesion surface was not always fulfilled. To offset this effect, summation of MR images (Matlab, 2012b) to display a greater portion of the markers on a single image was possible and facilitated the selection of the 'control points'. In addition to the aspects already mentioned in this preliminary manual registration approach, the user-dependency, particularly the manual selection of control points, may also have contributed to the final fiducial registration error.

4.5. Advantages, limitations and future applications

Feasibility assessment of the external fiducial markers and corresponding visualisation technique revealed that despite the manual processes involved, this simple and cost-effective approach provided exceptional spatial accuracy for the co-registration of fiducial markers affixed to the thigh, a forensically relevant region especially in the investigation of sexual assault [5]. This study assessed a small subject group with specific inclusion criteria. An extensive evaluation of the visualisation of the externally visible soft tissue lesions in MRI and of the influence of size and location of such lesions on co-registration processes was beyond the scope of the present work. Furthermore, additional research is required to investigate the applicability of the markers to soft tissue lesions in corporal regions other than the thigh and to optimise the visualisation framework (e.g. automated marker detection and co-registration). The potential application of the proposed approach to address clinical needs, for example in dermatological examinations, including biopsies, also requires further research.

5. Conclusions

The combination of non-invasive corn oil based strand-shaped fiducial skin markers, the use of TIRM (TI = 200 ms) and TSE2D (SPAIR fat-suppression) imaging sequences and an affine transformation process provided a simple, cost-effective means by which to co-register photographs and MRI data from manually specified 'control points'. These markers enabled the co-registration of digital photographs and MR images of the thigh with high spatial accuracy (minimal fiducial registration error) in ten volunteers. Further investigation of the novel fiducial markers and visualisation approach assessed could bring improvements to not only the forensic documentation of soft tissue lesions, but also to clinical applications such as in the field of dermatology.

Acknowledgments

This work was partly supported by the province of Styria ("Land Steiermark") under the funding scheme 'HTI:Tech_for_Med' (ABT08-22-T-7/2013-13).

References

[1] O.M. Navarro, E.E. Laffan, B-Y. Ngan, Pediatric soft-tissue tumors and pseudotumors: MR imaging features with pathologic correlation, RadioGraphics 29 (2009) 887–906.
[2] American College of Radiology. ACR–SSR Practice Guideline for the Performance and Interpretation of Magnetic Resonance Imaging (MRI) of Bone and Soft Tissue Tumors; 2010.
[3] K. Yen, P. Vock, B. Tiefenthaler, G. Ranner, E. Scheurer, M.J. Thali, et al., Virtopsy: forensic traumatology of the subcutaneous fatty tissue; multislice computed tomography (MSCT) and magnetic resonance imaging (MRI) as diagnostic tools, J. Forensic Sci. 49 (2004) 799–806.
[4] J.V. Hajnal, D.L.G. Hill, D.J. Hawkes, Medical Image Registration, CRC Press, 2001.
[5] L. Bowyer, M.E. Dalton, Female victims of rape and their genital injuries, Brit. J. Obstetr. Gynaecol. 104 (1997) 617–620.
[6] A.M. DeSchepper, F. Vanhoenacker, J. Gielen, P.M. Parizel, Imaging of Soft Tissue Tumors, 3rd ed., Springer-Verlag, Germany, 2006.
[7] T.S. Tsai, H.A. Evans, L.F. Donnelly, G.S. Bisset, K.H. Emery, Fat necrosis after trauma: a benign cause of palpable lumps in children, Am. J. Roentgenol. 169 (1997) 1623–1626.
[8] J.W. Gilbert, G.R. Wheeler, G.B. Richardson, S.L. Herder, G.E. Mick, E. Watts, et al., Guidance of magnetic resonance imaging and placement of skin-marker localization devices, J. Neurosurg. Sci. 55 (2011) 85–88.
[9] S.K. Rosahl, A. Gharabaghi, T. Liebig, C.D. Feste, M. Tatagiba, M. Samii, Skin markers for surgical planning for intradural lesions of the thoracic spine: technical note, Surg. Neurol. 58 (2002) 346–348.
[10] A.D. Ward, C. Crukley, C.A. McKenzie, J. Montreuil, E. Gibson, C. Romagnoli, et al., Prostate: registration of digital histopathologic images to in vivo MR images acquired by using endorectal receive coil, Radiology 263 (2012) 856–864.
[11] K. Ogris, E. Hassler, A. Petrovic, B. Neumayer, T. Widek, E. Scheurer, Evaluation of impact factors in the regeneration process of hematomas in the subcutaneous fatty tissue, International Society for Magnetic Resonance in Medicine, Milan, 2014p. 2265.
[12] K. Ogris, M. Urschler, A. Petrovic, K. Yen, E. Scheurer, Artificial hematomas in subcutaneous fatty tissue: volume estimation by using different MR sequences and manual segmentation of pork belly phantoms, International Society for Magnetic Resonance in Medicine, Montreal, 2011p. 2581.
[13] J. Ren, I. Dimitrov, A.D. Sherry, C.R. Malloy, Composition of adipose tissue and marrow fat in humans by 1H NMR at 7 Tesla, J. Lipid Res. 49 (2008) 2055–2062.
[14] Belitz H, Grosch W. Quimica de los Alimentos. 2nd ed. Zaragoza: Acribia; 1997.
[15] M. Urschler, J. Höller, A. Bornik, T. Paul, M. Giretzlehner, H. Bischof, et al., Intuitive presentation of clinical forensic data using anonymous and person-specific 3D reference manikins, Forensic Sci. Int. 241 (2014) 155–166.